Sensitivity of the Ocean State to the Vertical Distribution of Internal-Tide-Driven Mixing

ANGELIQUE MELET

Geophysical Fluid Dynamics Laboratory, Princeton University, Princeton, New Jersey

ROBERT HALLBERG

National Oceanic and Atmospheric Administration/Geophysical Fluid Dynamics Laboratory, Princeton, New Jersey

SONYA LEGG

Geophysical Fluid Dynamics Laboratory, Princeton University, Princeton, New Jersey

KURT POLZIN

Woods Hole Oceanographic Institution, Woods Hole, Massachusetts

(Manuscript received 19 March 2012, in final form 21 November 2012)

ABSTRACT

The ocean interior stratification and meridional overturning circulation are largely sustained by diapycnal mixing. The breaking of internal tides is a major source of diapycnal mixing. Many recent climate models parameterize internal-tide breaking using the scheme of St. Laurent et al. While this parameterization dynamically accounts for internal-tide generation, the vertical distribution of the resultant mixing is ad hoc, prescribing energy dissipation to decay exponentially above the ocean bottom with a fixed-length scale. Recently, Polzin formulated a dynamically based parameterization, in which the vertical profile of dissipation decays algebraically with a varying decay scale, accounting for variable stratification using Wentzel–Kramers–Brillouin (WKB) stretching. This study compares two simulations using the St. Laurent and Polzin formulations in the Climate Model, version 2G (CM2G), ocean–ice–atmosphere coupled model, with the same formulation for internal-tide energy input. Focusing mainly on the Pacific Ocean, where the deep low-frequency variability is relatively small, the authors show that the ocean state shows modest but robust and significant sensitivity to the vertical profile of internal-tide-driven mixing. Therefore, not only the energy input to the internal tides matters, but also where in the vertical it is dissipated.

1. Introduction

Diapycnal mixing plays a key role in maintaining the ocean stratification and meridional overturning circulation. Away from the surface layers, several processes contribute to diapycnal mixing, such as shear instabilities (e.g., Alford and Pinkel 2000), overflows (e.g., Legg et al. 2009), or mixing hydraulic jumps (Thurnherr et al. 2005) but in the ocean interior, it is largely sustained by breaking internal waves. Important sources of energy for internal waves are winds, leading to the generation of near inertial waves (e.g., D'Asaro et al. 1995; Alford 2001, 2003), and the flow of sub- and near-inertial currents and barotropic tides over topography in the stratified ocean, leading to, respectively, the generation of internal lee waves (e.g., Nikurashin and Ferrari 2011) and baroclinic tides (internal waves at the tidal frequency, also called internal tides, e.g., Egbert and Ray 2000; Niwa and Hibiya 2001; Garrett and Kunze 2007). Once generated, internal waves transport mechanical energy in the ocean. Part of this energy is dissipated locally, near the generation site, while the remainder propagates away in the form of low-mode internal waves (Alford and Zhao 2007). Among the different classes of internal waves, baroclinic tides are especially important since it has been

Corresponding author address: Angelique Melet, Geophysical Fluid Dynamics Laboratory, Princeton University, 201 Forrestal Road, Princeton, NJ 08540-6649.
E-mail: angelique.melet@noaa.gov

DOI: 10.1175/JPO-D-12-055.1

estimated that their breaking provides half the 2 terrawatts (TW) necessary to maintain the thermohaline circulation (e.g., Munk and Wunsch 1998; Egbert and Ray 2001; Jayne and St. Laurent 2001).

The breaking of internal waves occurs on scales too small to be resolved explicitly in ocean climate models. Physically based parameterizations of the small-scale mixing induced by internal waves, and in particular by baroclinic tides, are crucial for realistic simulation of the thermohaline circulation, transport and storage of heat and carbon dioxide (e.g., Wunsch and Ferrari 2004; Jayne 2009; Friedrich et al. 2011), centennial- to millennial-scale variability, and for estimating how mixing might change in a changing ocean. Such parameterizations need to incorporate current understanding of the transfer of energy from barotropic to baroclinic tides, as well as representing the less well understood processes by which the internal tides break and dissipate (St. Laurent and Garrett 2002). Traditionally, diapycnal mixing was parameterized in ocean models by a constant diffusivity or a horizontally uniform vertical profile of diffusivity (e.g., Bryan and Lewis 1979; Huang 1999). More recently, the parameterization developed by St. Laurent et al. (2002) has been commonly implemented in ocean models to take into account the diapycnal mixing caused by dissipation of internal tides near their generation site. In this semiempirical, energetically constrained parameterization, dissipation is bottom enhanced, as in the observations (Polzin et al. 1997; Ledwell et al. 2000). While the energy flux into the baroclinic tide is based on the internal-tide generation linear theory of Bell (1975), the subsequent dissipation of this energy remains ad hoc, with an arbitrarily prescribed exponential vertical decay. The fraction of energy dissipated locally is set uniformly to 1/3, matching observations from a single location. Recently, Polzin (2009) formulated a more dynamically based parameterization of internal-tide driven mixing, based on a radiation balance equation (Polzin 2004), which links the dissipation profile associated with internal breaking to the finescale internal wave shear producing that dissipation. The vertical profile of internal-tide driven energy dissipation can then vary in time and space, and evolve in a changing climate.

Here, we examine the sensitivity of the ocean state to the vertical profile of tidal energy dissipation by comparing two simulations of a global ocean–ice–atmosphere coupled model, employing the Polzin (2009) formulation and St. Laurent et al. (2002) parameterization, respectively. We focus mainly on the Pacific Ocean, where numerous internal-tide generation sites are found, and where the deep ocean is less prone to low-frequency variability than the Atlantic Ocean, yielding a favorable signal to noise ratio.

2. Tidally driven mixing parameterizations

a. St. Laurent et al. (2002) parameterization

In this parameterization, first implemented in an ocean general circulation model (OGCM) by Simmons et al. (2004) and subsequently by many others (e.g., Saenko and Merryfield 2005; Bessières et al. 2008; Jayne 2009), the turbulent dissipation rate of internal tide energy ϵ is expressed as

$$\epsilon = \frac{qE(x,y)}{\rho} F(z), \tag{1}$$

with ρ the density of seawater, $E(x, y)$ the energy flux per unit area transferred from barotropic to baroclinic tides, q the fraction of internal-tide energy dissipated locally, and $F(z)$ the vertical structure of the dissipation.

The term $E(x, y)$ is given by the Jayne and St. Laurent (2001) formulation, based on a simple scale relation consistent with a linear theory of internal-tide generation (Bell 1975):

$$E(x,y) = (1/2)\rho_0 N_b \kappa h^2 \langle U^2 \rangle, \tag{2}$$

with the following parameters: ρ_0 is the reference density of seawater, N_b is the buoyancy frequency along the seafloor, κ and h are the wavenumber and amplitude scales for the topographic roughness, and $\langle U^2 \rangle$ is the barotropic tide variance.

The term $F(z)$ is specified to give exponential decay of ϵ above topography and unit integral over the whole depth to satisfy energy conservation:

$$F(z) = \frac{e^{-z/z_s}}{z_s(1 - e^{-H/z_s})}, \tag{3}$$

with z the height above the seafloor, z_s a constant decay scale, and H the total ocean depth.

b. Polzin (2009) based parameterization

1) POLZIN'S FORMULATION

The parameterization of Polzin (2009) links the energy dissipation profile to the finescale internal wave shear producing that dissipation, using an idealized vertical wavenumber energy spectrum to identify analytic solutions to a radiation balance equation (Polzin 2004). These solutions yield a dissipation profile $\epsilon(z)$:

$$\epsilon = \frac{\epsilon_0}{[1 + (z/z_p)]^2}, \tag{4}$$

where the magnitude ϵ_0 and scale height z_p can be expressed in terms of the spectral amplitude and bandwidth

of the idealized vertical wavenumber energy spectrum in uniform stratification (Polzin 2009).

To take into account the nonuniform stratification, Polzin (2009) applied a buoyancy scaling using the Wentzel–Kramers–Brillouin (WKB) approximation. As a result, the vertical wavenumber of a wave packet varies in proportion to the buoyancy frequency N, which in turn implies an additional transport of energy to smaller scales, and thus a possible enhanced mixing in regions of strong stratification. Such effects can be described by buoyancy scaling the vertical coordinate z as

$$z^*(z) = \int_0^z \left[\frac{N^2(z')}{N_b^2}\right] dz', \tag{5}$$

with z' being positive upward relative to the bottom of the ocean. The turbulent dissipation rate then becomes

$$\epsilon = \frac{\epsilon_0}{[1 + (z^*/z_p)]^2}\frac{N^2(z)}{N_b^2}. \tag{6}$$

The spectral amplitude and bandwidth of the idealized vertical wavenumber energy spectrum are identified after WKB scaling using a quasi-linear spectral model of internal-tide generation that incorporates horizontal advection of the barotropic tide into the momentum equation (Bell 1975). As a result, Polzin's formulation leads to an expression for the spatially and temporally varying dissipation of internal tide energy at the bottom ϵ_0, and vertical scale of decay for the dissipation of internal tide energy z_p.

2) IMPLEMENTATION OF POLZIN'S FORMULATION

(i) Energy-conserving form

To satisfy energy conservation (the integral of the vertical structure for the turbulent dissipation over depth should be unity), the dissipation is rewritten as

$$\epsilon = \frac{\epsilon_0 z_p}{[1 + (z^*/z_p)]^2}\frac{N^2(z)}{N_b^2}\left[\frac{1}{z^*(z = H)} + \frac{1}{z_p}\right]. \tag{7}$$

The power input E from the barotropic to baroclinic tides derived from Polzin's parameterization differs from the one derived from the theory of Bell (1975) and used in Simmons et al. (2004). In our implementation, unlike Polzin's original formulation, we use the St. Laurent et al. (2002) template for the vertical flux of energy at the ocean floor, so that in both the Simmons and the Polzin formulations:

$$\int_0^H \epsilon(z)\, dz = \frac{qE}{\rho}. \tag{8}$$

Whereas Polzin (2009) assumed that the total dissipation was locally in balance with the barotropic to baroclinic energy conversion rate ($q = 1$), here we use the Simmons value of $q = 1/3$ to retain as much consistency as possible between both parameterizations, and to allow a more direct comparison between the effects of the vertical structure.

(ii) Vertical decay-scale reformulation

We follow the Polzin (2009) prescription for the vertical scale of decay for the dissipation of internal-tide energy. However, we assume that the topographic power law, denoted as ν in Polzin (2009), is equal to 1 (instead of 0.9) and we reformulated the expression of z_p to put it in a more readable form:

$$z_p = \frac{z_p^{\mathrm{ref}}(\kappa^{\mathrm{ref}})^2(h^{\mathrm{ref}})^2(N_b^{\mathrm{ref}})^3}{U^{\mathrm{ref}}}\frac{U}{h^2\kappa^2 N_b^3}. \tag{9}$$

The superscript ref refers to reference values of the various parameters, as given by observations from the Brazil basin. Therefore, (9) can be rewritten as

$$z_p = \mu(N_b^{\mathrm{ref}})^2\frac{U}{h^2\kappa^2 N_b^3}, \tag{10}$$

where μ is a nondimensional constant ($\mu = 0.069\,70$) and $N_b^{\mathrm{ref}} = 9.6\ 10^{-4}\ s^{-1}$. Finally, a minimum decay scale of $z_p = 100$ m is imposed in our implementation.

(iii) Reformulation of the WKB scaling

Since the dissipation is expressed as a function of the ratio z^*/z_p, a different WKB scaling can be used so long as we modify z_p accordingly. In the implemented parameterization, we define the scaled height coordinate z^* by

$$z^*(z) = \frac{1}{\overline{N^2(z)}^z}\int_0^z N^2(z')\, dz', \tag{11}$$

with z' defined to be the height above the ocean bottom. By normalizing N^2 by its vertical mean $\overline{N^2}^z$, z^* ranges from 0 to H, the depth of the ocean.

The WKB-scaled vertical decay scale for the Polzin formulation becomes

$$z_p^* = \mu(N_b^{\mathrm{ref}})^2\frac{U}{h^2\kappa^2 N_b\overline{N^2}^z}. \tag{12}$$

Unlike the St. Laurent et al. (2002) parameterization, the vertical decay scale now depends on physical variables and can evolve with a changing climate.

Finally, the Polzin vertical profile of dissipation implemented in the model is given by

$$\epsilon = \frac{qE(x,y)}{\rho[1+(z^*/z_p^*)]^2}\frac{N^2(z)}{\overline{N^2}^z}\left(\frac{1}{H}+\frac{1}{z_p^*}\right). \quad (13)$$

In both the Simmons and the Polzin formulation, turbulent diapycnal diffusivities are inferred from the dissipation ϵ using the Osborn (1980) model:

$$k_d = \frac{\Gamma\epsilon}{N^2}. \quad (14)$$

The mixing efficiency Γ is generally set to 0.2 (Osborn 1980). However, here we use

$$\Gamma = 0.2\frac{N^2}{N^2+\Omega^2}, \quad (15)$$

where Ω is the angular velocity of the Earth, so that buoyancy fluxes tend to zero in regions of very weak stratification, including in a well-mixed bottom boundary layer, allowing a no-flux bottom boundary condition to be satisfied.

Our study therefore compares the ocean state in two simulations differentiated only by their vertical profile of dissipation: one using the Simmons exponentially decaying tidal energy profile with a fixed decay scale (set to z_s = 300 m; St. Laurent and Nash 2004), the other using the Polzin algebraically decaying profile with a spatially and temporally varying decay scale.

3. Model description

The two parameterizations are implemented in the Geophysical Fluid Dynamics Laboratory (GFDL) Climate Model, version 2 [with Generalized Ocean Layer Dynamics (GOLD) ocean component] (CM2G), ocean–ice–atmosphere coupled model, used for the Intergovernmental Panel on Climate Change (IPCC) Fifth Assessment Report (AR5) suite (Dunne et al. 2012). The ocean component is the GOLD isopycnal model (Hallberg and Adcroft 2009). The zonal resolution is 1°. The meridional resolution is 1° in the midlatitudes from 20° to 60°, and it increases toward ½° poleward of 60° and toward ⅓° equatorward of 20°. Sixty-three vertical layers are used as follows: 59 in the ocean interior, 2 for the mixed layer, and 2 additional buffer layers for smooth water mass exchange with the isopycnal interior. The isopycnal coordinate allows the model to represent the largely adiabatic interior of the ocean more naturally, and diapycnal mixing is explicitly parameterized. In addition to the tidal mixing parameterization, parameterizations of diapycnal mixing caused by resolved shear (Jackson et al. 2008) and bottom friction (Legg et al. 2006) are also included, as well as a vertically uniform latitude-dependent background diffusivity, which attempts to account for other sources of mixing (Harrison and Hallberg 2008). The absence of spurious mixing associated with advection in the isopycnal coordinates (Griffies et al. 2000; Ilicak et al. 2012) facilitates study of the effects of changing the diapycnal mixing parameterization. Along-isopycnal tracer mixing is implemented through a Laplacian operator, while the horizontal viscosity uses a combination of Laplacian and biharmonic operators.

The tidal mixing parameterization uses barotropic tidal velocities computed with 8 major tidal components by the Oregon State tidal model (Egbert and Erofeeva 2002), and topographic roughness amplitudes and wavenumbers computed from the bathymetric dataset of Smith and Sandwell (1997).

The simulation using the algebraically decaying vertical function is referred to as the Polzin simulation (PS) hereafter, while the simulation using the exponential decay vertical function is referred to as the Simmons simulation (SS). The models were integrated for 1000 years from climatological conditions (Levitus et al. 1998, for the ocean state) using the radiative forcing of the year 1990. Results are shown for the mean of the last century of the 1000-yr simulations, but are similar to other centuries late in the simulations.

4. Results

The climate model used in this study is drifting from its initial state over time, but the ocean state has reached a quasi equilibrium by the end of the 1000-yr simulations (Fig. 1). This drift can mainly be explained by two factors. First, in the standard CM2G simulations (Dunne et al. 2012), mixing is increased above the level predicted from the tidal mixing parameterization by adding ad hoc mixing (intended to take into account other sources of mixing) with the parameterization proposed by Gargett (1984). To study the sensitivity of the ocean state to the vertical profile of the local dissipation of internal tides, this additional source of mixing is removed from the simulations in this study, and so the total diapycnal diffusivities in our simulations are comparatively low. Second, since the observed state of the ocean in 1990 that is used for the model initial conditions is not in balance with the 1990 radiative forcing, the prescription of the atmospheric radiative forcing of year 1990 in our ocean–atmosphere coupled simulations leads to a global committed warming of the ocean over time. For these reasons, the simulations presented in this study tend to equilibrate toward an ocean state that is slightly different from the contemporary one. Therefore, comparison of our simulations with observations

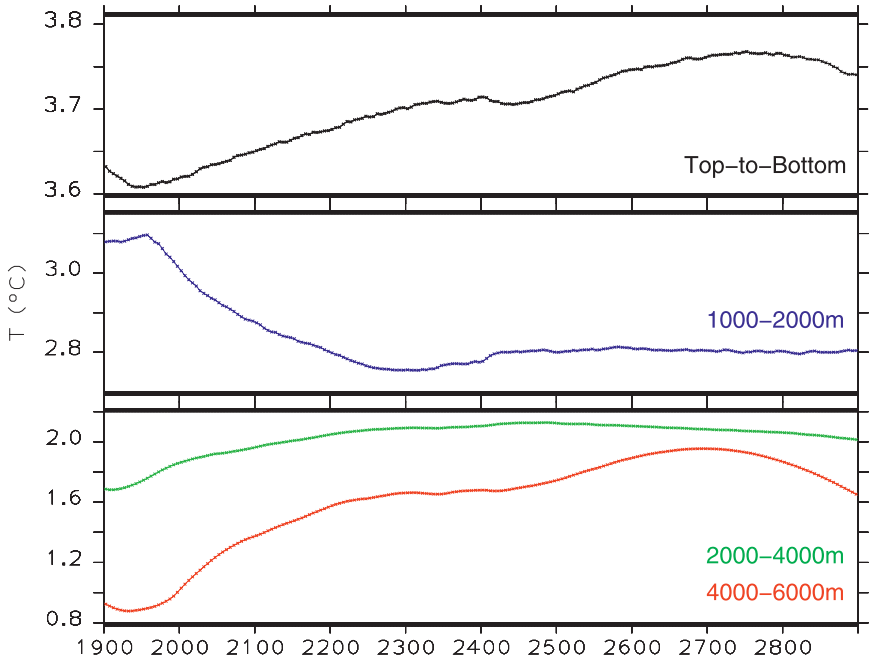

FIG. 1. Time series of the mean global ocean temperature from 5-yr means in the Polzin simulation for different vertical layers: total water column (black line), 1000–2000 m (blue line), 2000–4000 m (green line), and 4000–6000 m bottom (red line).

to evaluate which vertical profile of the local dissipation of internal tides is more realistic is not fully relevant.

The energy input into internal tides (1.41 TW, global ocean; 0.60 TW, Pacific) is similar (within 3%) in both simulations. The conversion of turbulent kinetic energy into potential energy through internal-tide mixing, defined as

$$P = \int \rho \epsilon \, dV = \frac{1}{\Gamma} \int \rho K_{d,\mathrm{tidal}} N^2 \, dV, \qquad (16)$$

is also similar (within 1.5%) in both simulations, with values of 0.42 TW for the global ocean, and 0.18 TW for the Pacific Ocean. Therefore, the principal difference between PS and SS is the vertical distribution of this mixing.

Whereas the vertical decay scale is uniformly set to 300 m in SS, the vertical decay scale z_p used in PS exhibits strong spatial variability (Fig. 2a). In particular, it tends to be smaller in regions of strong conversion of barotropic to baroclinic tide energy (Fig. 2b). Physically, this could be related to the spectral amplitudes of the shear spectrum. Indeed, the nonlinear propagation model of Polzin (2004) casts nonlinearity as an energy cascade and balances this cascade with an energy flux convergence, which appears as turbulent dissipation. The vertical decay scale that comes from this scheme, (9), depends on several parameters, among which the spectral amplitudes of the shear spectrum is thought to play a major role in explaining the shorter decay scale in regions of strong barotropic to baroclinic tidal energy conversion. The greater the spectral amplitudes of the shear spectrum, the greater the nonlinearity and the nonlinear transports. To the degree that stronger barotropic to baroclinic conversion implies higher spectral levels of shear, stronger conversion means greater nonlinearity and a shorter vertical decay scale.

In our simulations, tidally driven diapycnal diffusivities are the main contribution to the total diapycnal diffusivities in the ocean interior (not shown). The algebraic decay of tidal energy dissipation in PS leads to more dissipation occurring higher in the water column than in SS with exponential decay (Fig. 3, black and blue curves). As a result, tidally induced diapycnal diffusivities tend to be weaker in the deep ocean in PS, while they are stronger in the lower thermocline (Fig. 4a). These patterns are robust across the majority of the World Ocean (Figs. 4b,c), although in regions of short decay scale z_p in PS (often associated with strong barotropic to baroclinic tidal energy conversion), tidally induced diapycnal diffusivities can be stronger in the deep ocean (2000–4000 m) in PS than in SS (Fig. 4c).

In the approximation of a linear equation of state, the temporal tendency of the ocean buoyancy B from tidal mixing is related to the vertical gradient of the tidal energy dissipation ϵ by:

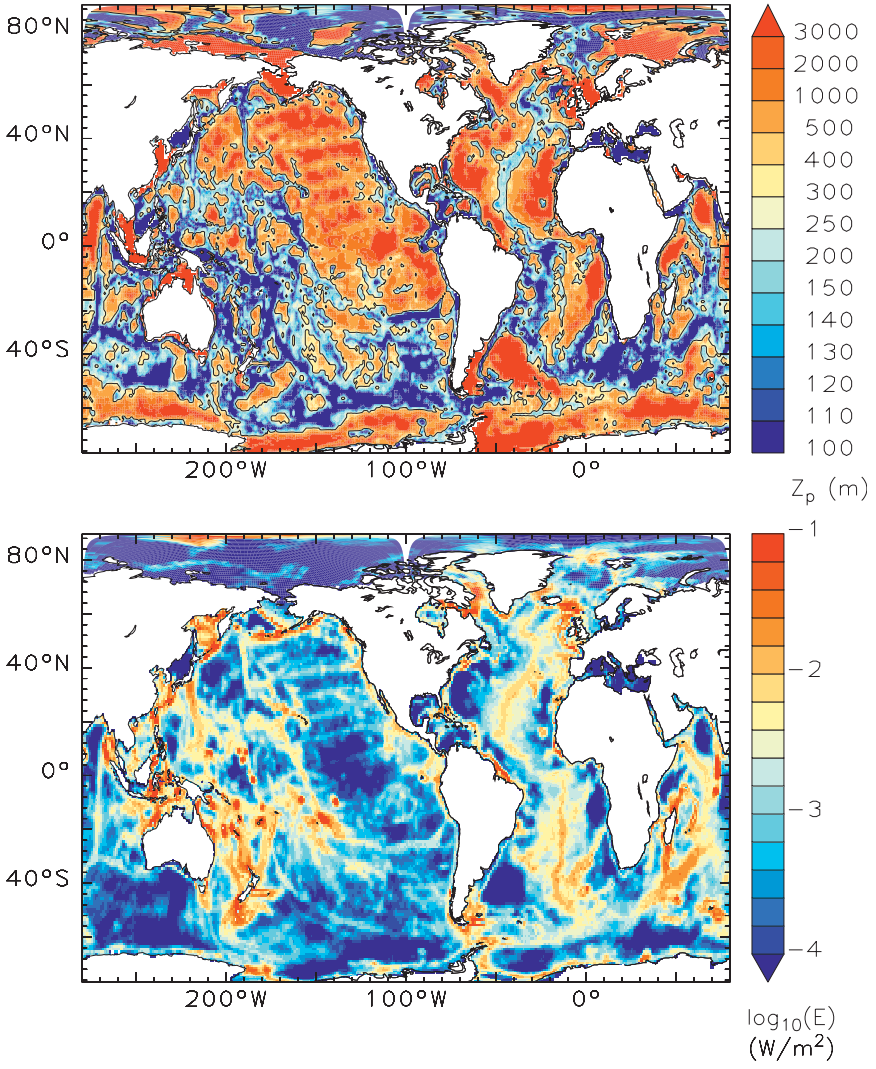

FIG. 2. (top) Vertical decay scale z_p (m) and (bottom) conversion of barotropic to baroclinic tide energy (logarithmic scale; W m^{-2}) in the Polzin simulation for years 901–1000.

$$\left(\frac{\partial B}{\partial t}\right)_{\text{tidal}} = -\frac{g}{\rho_0}\left(\frac{\partial \rho}{\partial t}\right)_{\text{tidal}} = \frac{\partial(\Gamma\epsilon)}{\partial z}. \qquad (17)$$

Although the model uses a fully nonlinear equation of state, (17) is useful for understanding the model's results. The no-flux bottom boundary condition for buoyancy ($\Gamma = 0$) leads to a positive vertical gradient of $\Gamma\epsilon$ over a thin homogenized bottom boundary layer, resulting in a lightening of waters. In the remaining water column above, the vertical gradient of the energy dissipation in SS is negative (Fig. 3, blue curve), leading to denser waters. The same would be true in PS without WKB scaling (Fig. 3, red curve), although the algebraic vertical decay of energy leads to a more broadly distributed decrease above the bottom boundary layer. When the variable stratification is accounted for in PS, the vertical gradients of energy dissipation can change sign several times over the water column (Fig. 3, black curve). Therefore, buoyancy can now also increase higher in the water column where the stratification is enhanced (as in the lower thermocline, Fig. 3, green curve).

Examination of the differences in temperature and density between PS and SS shows that these predictions for the buoyancy modification are supported by the model integrations (Fig. 5). The most significant signal is found in the lower thermocline, between roughly 1000 and 2000 m, where the stratification is stronger than in the deep ocean (Fig. 5, left), and waters warm significantly in PS relative to SS (Fig. 5, middle). In the Southern Ocean, this relative warming is mainly found equatorward of 50°S, where the water column gets

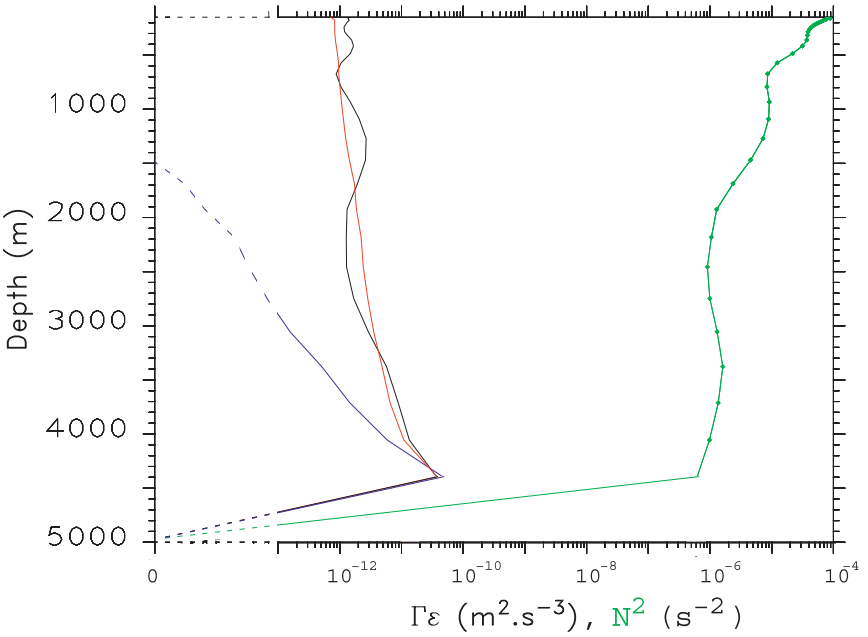

FIG. 3. Vertical profile of tidal energy dissipation ϵ (m^2 s^{-3}) times the dissipation efficiency Γ, averaged over the first year at 26°S, 155°W for the Simmons simulation (blue), the Polzin simulation without WKB scaling (red), and the Polzin simulation with WKB scaling (black). The corresponding Polzin WKB simulation squared buoyancy frequency N^2 (s^{-2}) vertical profile is shown in green. The depth integral of the tidal energy dissipation is equal to the same constant (qE/ρ) in the three cases. The horizontal axis is logarithmic, but goes to zero to reflecting the no buoyancy flux condition at the bottom of the ocean. Therefore, the x axis is distorted between 0 and 10^{-13}, and values of $\Gamma\epsilon$ and N^2 lower than 10^{-13} are presented with dashed lines.

stratified deeper in the ocean (above roughly 2500 m, Fig. 5d, middle). In the quiescent Pacific and Indian Oceans, these differences of temperature are accumulating quite linearly in time (Figs. 5a,b, right) until a quasi equilibrium is reached (after ~7 centuries of model integration). The corresponding difference of temperature over the last century of the simulation is 0.06°C for the Pacific Ocean and 0.11°C for the Indian Ocean. In the Atlantic and Southern Oceans, more variability is found but a clear warming is still observed, with a trend of 0.23°C/1000 yr for the 1000–2000-m layer of the Atlantic Ocean, and 0.09°C/1000 yr for the 1000–3000-m layer of the Southern Ocean.

These differences of temperature are robust spatially and in time (Fig. 6). Locally, differences of temperature at 1500 m can reach 0.15°C in the Pacific, 0.17°C in the Indian Ocean, while stronger differences of 0.5°–1°C can be locally found in the Atlantic Ocean and of ±0.25°C in the Southern Ocean. Below, between 2000- and 4000-m depth, a weaker difference in temperature exists, with slightly warmer water in PS relative to SS (Fig. 5). By the end of the 1000-yr simulations, the differences of temperature in this depth range have largely stabilized (Fig. 5, right). The corresponding differences of temperature over the last century of the simulations are 0.02°C for the Pacific Ocean, 0.015°C for the Indian Ocean, and 0.11°C for the Atlantic Ocean. Finally, although the ocean has not reached equilibrium in the deep layers below 4000-m depth (Fig. 1), the deep waters tend to get cooler in PS than in SS below 4000 m. In the Pacific and Indian Oceans, differences are weak, with trends of −0.01°C/1000 yr and −0.03°C/1000 yr, respectively. In the Southern and Atlantic Oceans, more variability and stronger signals are found, with a trend of −0.08°C/1000 yr and 0.08°C/1000 yr, respectively (Fig. 5).

The differences in the dissipation profiles also lead to a broader lower thermocline, shown for the Pacific Ocean in Fig. 7a. The stratification in PS is also stronger relative to SS below 1500 m, especially between roughly 1500- and 2500-m depth (Fig. 7b).

Using idealized simulations, Scott and Marotzke (2002) showed that the vertical structure of the turbulent dissipation profile is important in setting stratification and the overturning strength. Our realistic simulations show that indeed, the differences in the vertical distribution of tidal mixing lead to differences in the meridional overturning circulation (MOC). In the more quiescent Indo-Pacific Ocean, the MOC is weaker in PS

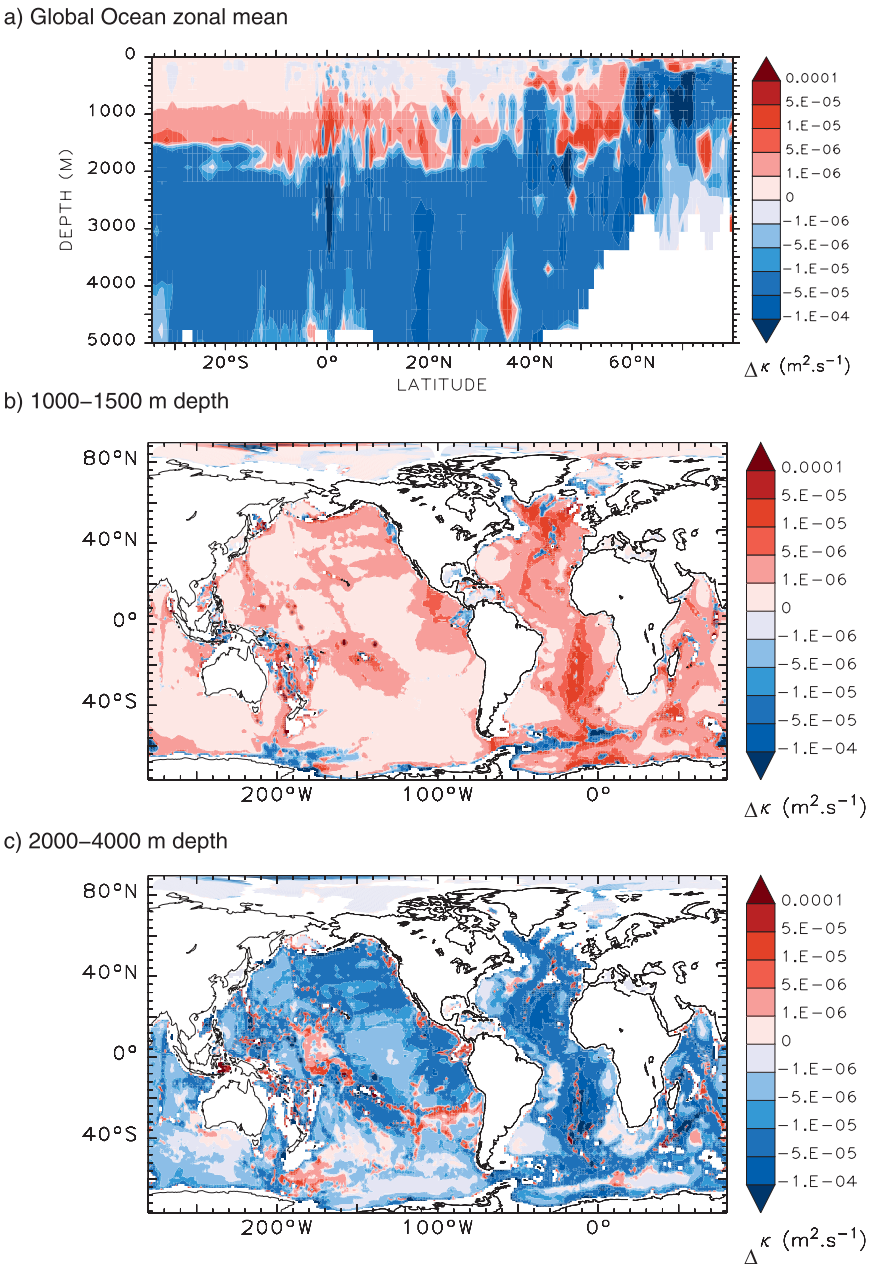

FIG. 4. Difference of diapycnal diffusivity driven by internal tides between the Polzin and Simmons simulations for years 901–1000 ($m^2\ s^{-1}$), (a) zonally averaged over the global ocean, (b) averaged over the 1000–1500-m-depth range, and (c) averaged over the 2000–4000-m-depth range.

than in SS, with differences in amplitude of roughly 10% (Fig. 8).

5. Conclusions and discussion

Dissipation of internal-tide energy is a major source of diapycnal mixing in the ocean, which plays a key role in maintaining the ocean stratification and meridional overturning circulation. While previous studies have largely focused on the conversion of energy from the barotropic to baroclinic tides, here we examine the sensitivity of the ocean state to the vertical profile of internal-tide energy dissipation, comparing two simulations of a global coupled ocean–ice–atmosphere model (CM2G) differing only in the formulation of this profile. The first uses an ad hoc uniform exponentially decaying

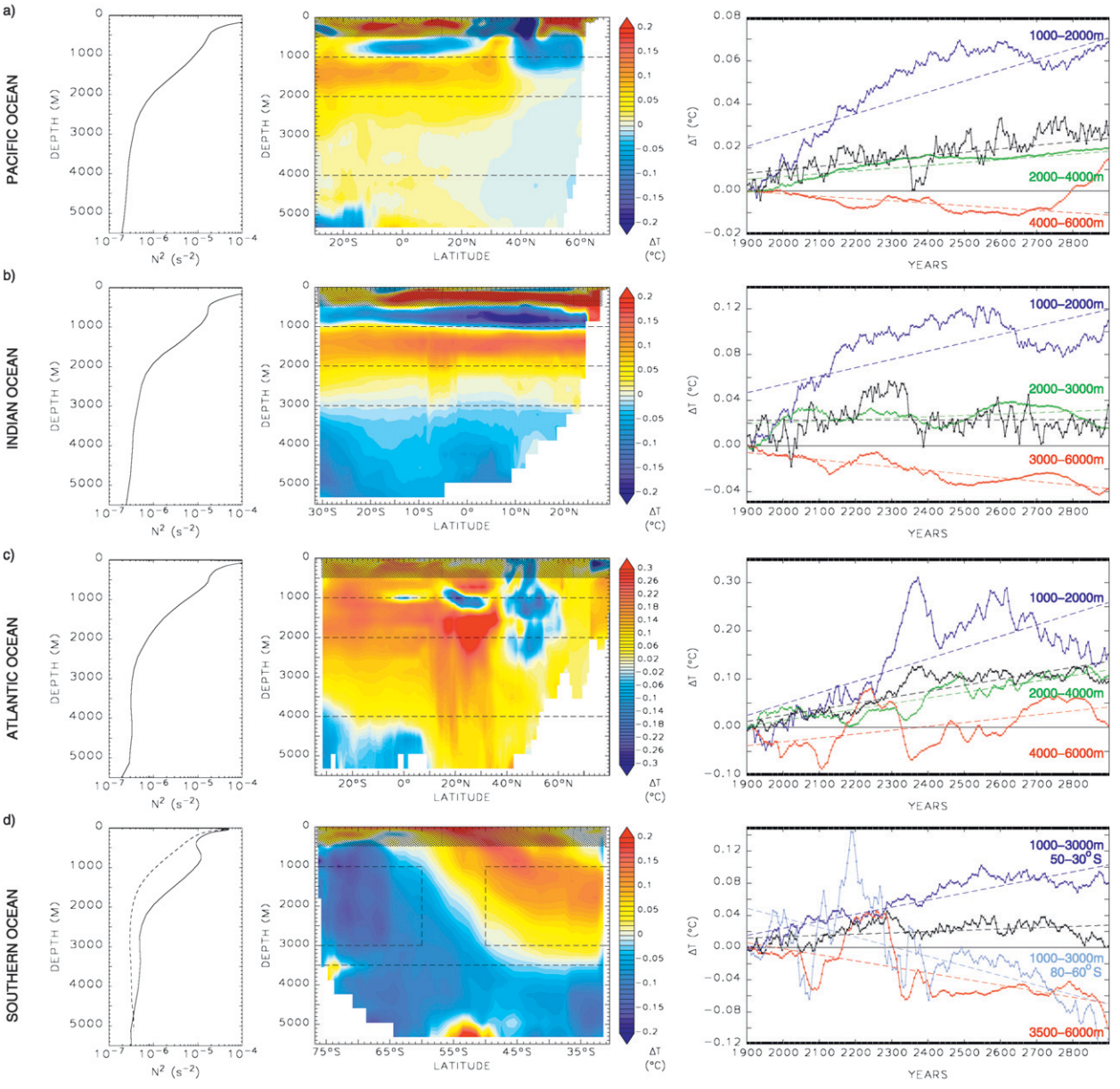

FIG. 5. (left) Basin mean buoyancy frequency profile (s^{-2}), (middle) zonally averaged difference in temperature (°C) between the Polzin and Simmons simulations by ocean basin, for years 901–1000. (right) Time series of the difference in the mean ocean basin temperature ΔT (°C) from 5-yr means between the Polzin and Simmons simulations for different vertical layers. The black line stands for the total water column. The colored lines show the different vertical layers indicated in the same color and delimited by dashed lines in the middle panels. The dashed lines in the right panels correspond to the linear regressions of the continuous lines. The different ocean basins are (a) Pacific Ocean, (b) Indian Ocean, (c) Atlantic Ocean, and (d) Southern Ocean. In the left panel of (d), the continuous line represents the mean buoyancy frequency profile (s^{-2}) averaged from 50° to 31°S while the dashed line represents the mean buoyancy frequency profile (s^{-2}) averaged from 77° to 60°S.

profile based on the St. Laurent et al. (2002) and Simmons et al. (2004) parameterization. In the second, we implemented a dynamically based vertical profile (Polzin 2009) where internal-tide dissipation decays algebraically from the bottom as a function of stratification, with a decay scale dependent on the ocean state. These two sensitivity simulations were run for 1000 years, until the sensitivity of the ocean state has reached a quasi equilibrium. This study does not aim at examining which vertical profile of the local dissipation of internal tides leads to the most realistic ocean state. We did not focus on possible reductions of model biases when using different vertical profile of the local dissipation of internal-tides, since impacts on model biases

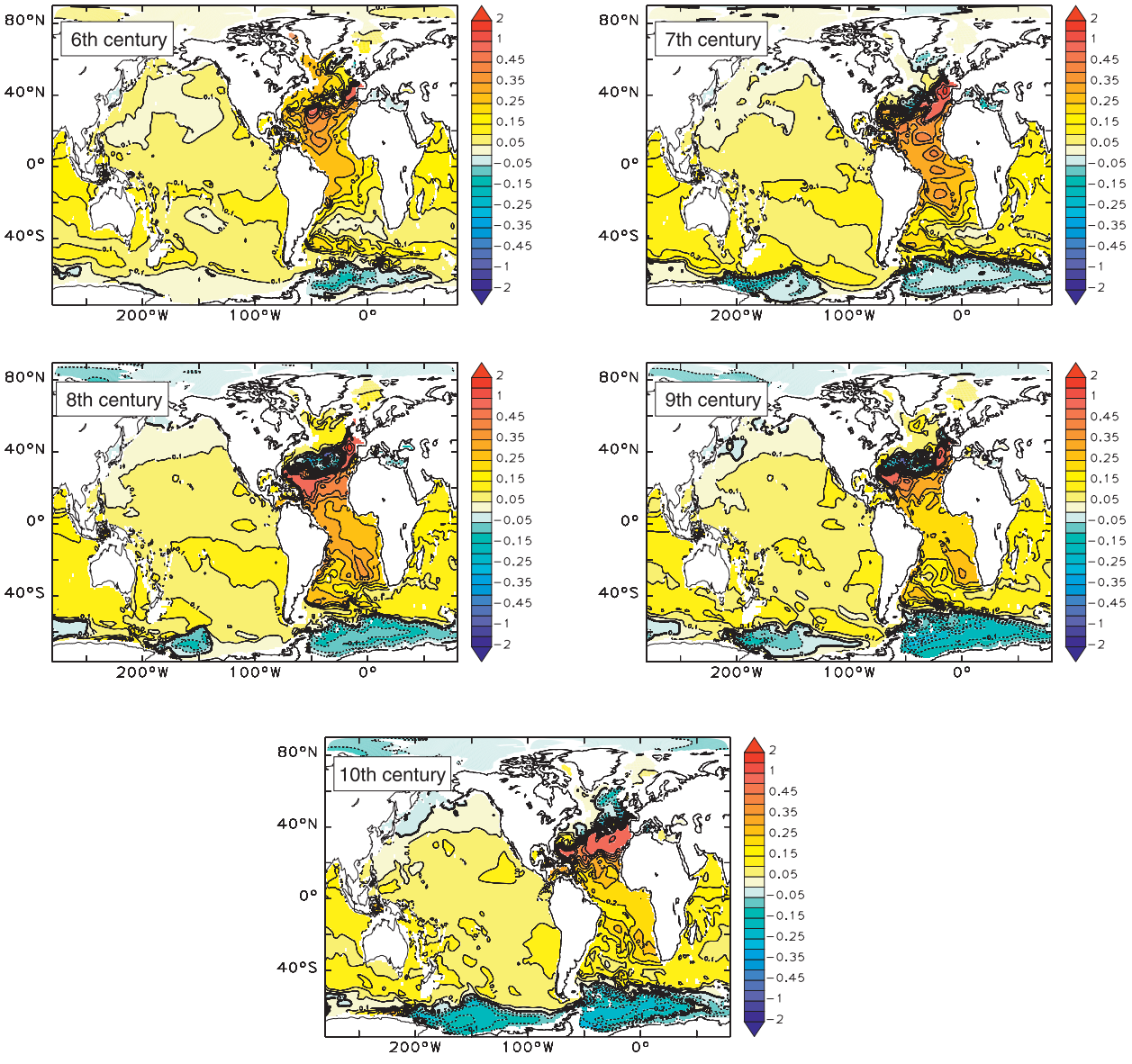

FIG. 6. Differences in temperature (°C) between the Polzin and Simmons simulations at 1500 m, averaged over each of the last 5 centuries of the simulations.

would be model-dependent. This study rather aimed at documenting the *sensitivity* of the ocean state to these vertical profiles of dissipation, which should be robust from one model to another.

We examined this sensitivity focusing on the Pacific Ocean where numerous internal-tide generation sites are found and large-scale advective variability is less pronounced than in other basins. The ocean state shows a well characterized and robust sensitivity: the most significant signal corresponds to a relative warming in the Polzin simulation in the lower part of the thermocline, hundreds to thousands of meters above the bottom, where the stratification increases relative to the deep ocean. The corresponding difference of temperature is the weakest over the Pacific Ocean, with a spatial average of 0.06°C, and the strongest in the Atlantic Ocean, where it can reach up to 1°C. As a result, a broadening of the lower thermocline is simulated in the Polzin simulation, together with an increase in abyssal stratification, which could influence the nutrient distribution and carbon budget of the ocean. The Indo-Pacific MOC is also sensitive to the vertical distribution of internal-tide driven mixing and is weaker in the Polzin simulation.

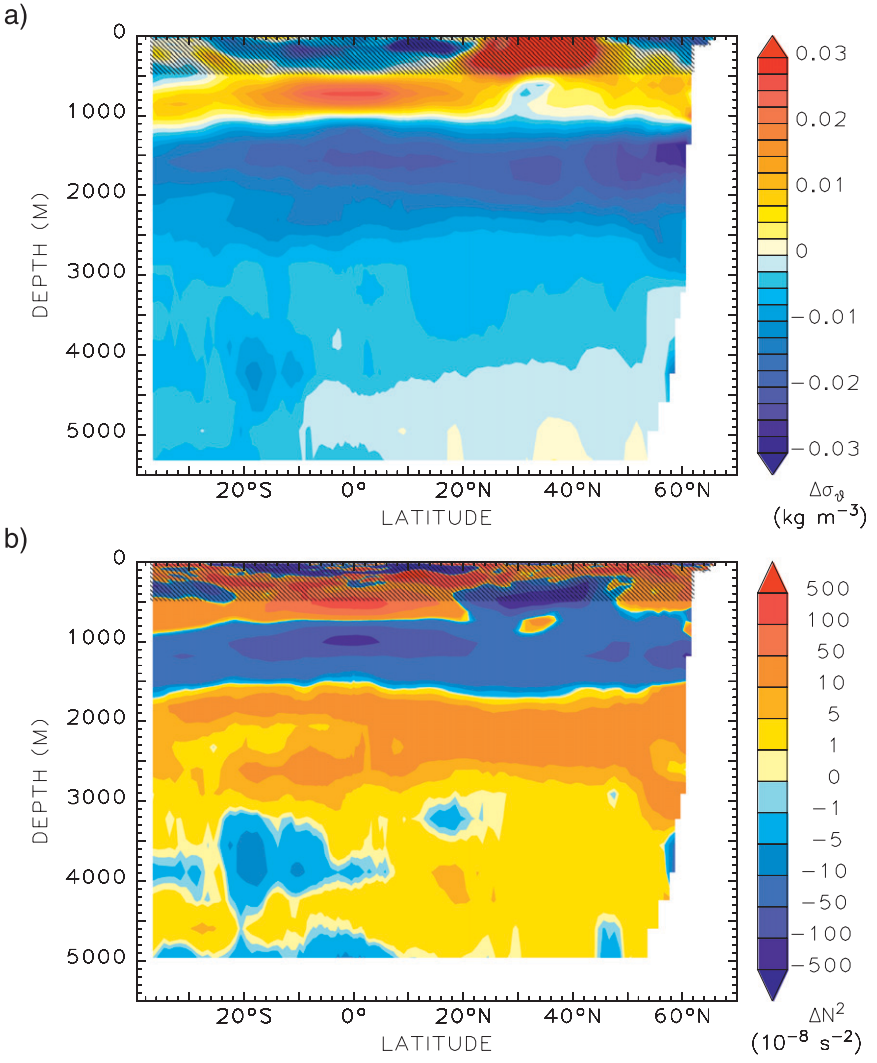

FIG. 7. (a) Difference in potential density (kg m^{-3}) and (b) squared buoyancy frequency (10^{-8} s^{-2}) between PS and SS zonally averaged over the Pacific Ocean and for years 901–1000.

Although robust and significant, the amplitude of the sensitivity is modest. Yet, the Polzin scheme has two main advantages compared to the Simmons: 1) it is more dynamically based and takes into account variable stratification, and 2) dissipation can evolve with a changing climate. Moreover, only a small fraction of internal-wave energy was taken into account in this study (⅓ of internal-tide energy), and the two vertical profiles were not dramatically different with enhanced dissipation above the ocean floor. The vertical structure of dissipation (e.g., WKB stretching) matters for other sources of internal waves too, and the sensitivity to the vertical profile of energy dissipation would be stronger if more energy dissipates in highly stratified regions such as the thermocline. Processes such as the dissipation of low-mode internal tides or parametric subharmonic instabilities (PSI, e.g., MacKinnon and Winters 2005) would also lead to enhanced dissipation in the thermocline. Therefore, this study represents a proof of concept that *not only the energy input to the internal tides matters, but also where in the vertical it is dissipated.*

The main objective of this study was not to implement the Polzin scheme in full. In particular, local hypsometry (Polzin 2009) was not taken into account and could impact the ocean state. This study is only a first step at improving the parameterization of internal-tide dissipation, and several uncertainties remain. Among them, the fraction of the internal-tide energy that dissipates locally q, held constant in this study, is likely to vary spatially and temporally. Current estimates of this fraction range from 10% to 40% (Klymak et al. 2006; St. Laurent and Nash 2004; Alford et al. 2011). Data

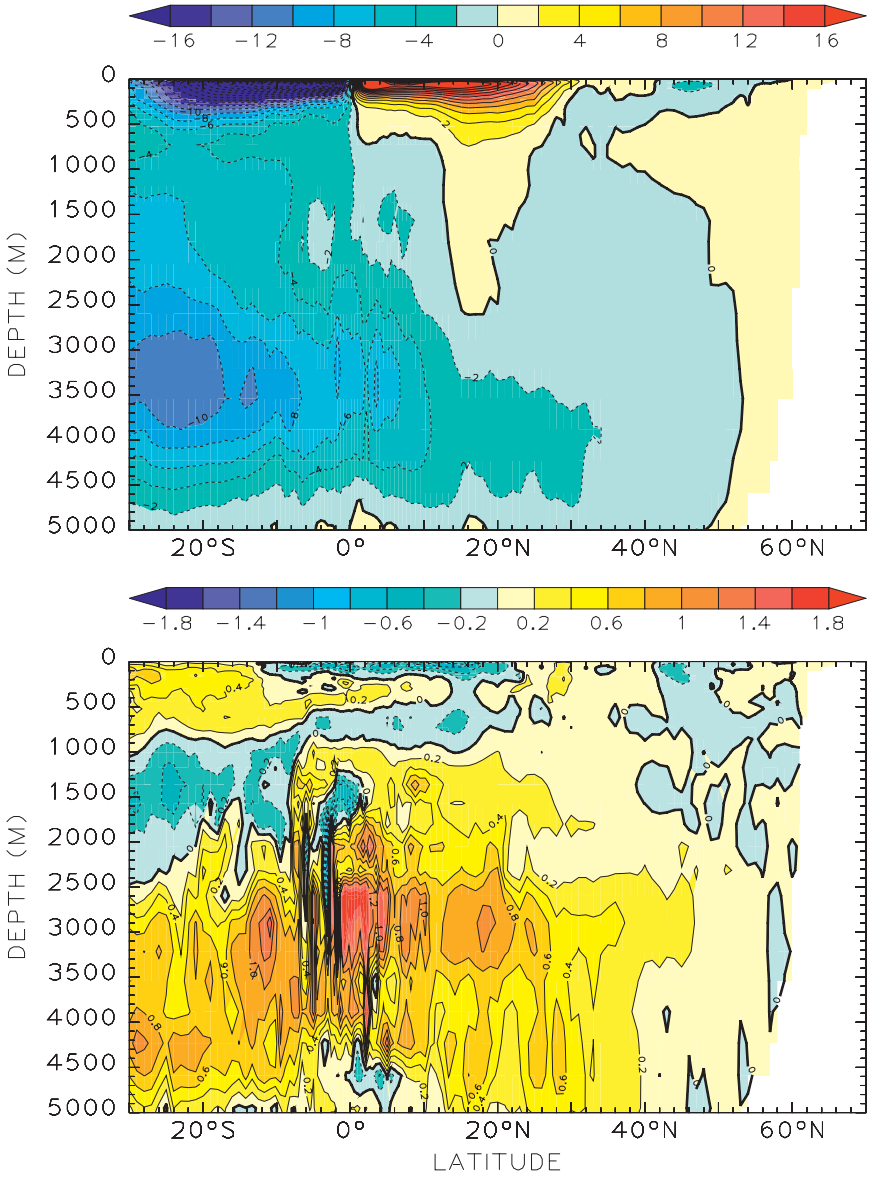

FIG. 8. (top) Indo-Pacific meridional overturning circulation (Sv; 1 Sv $\equiv 10^6$ m^3 s^{-1}) for the Polzin simulation for years 901–1000. (bottom) Differences in the Indo-Pacific meridional overturning circulation (Sv) between the Polzin and Simmons simulations for years 901–1000.

assimilation can be used to infer q (for the current ocean state, e.g., Melet et al. 2012) or high-resolution process simulations can be used to predict its dependence on parameters such as latitude (Nikurashin and Legg 2010), tidal velocity (Klymak et al. 2010), or topography.

This work is one component of the ongoing Internal Wave Driven Mixing Climate Process Team (CPT) collaboration, which aims at developing internal-wave-driven mixing parameterizations and evaluating their impacts in climate models. Ultimately, physically based parameterizations for the major processes contributing to ocean mixing through dissipation of internal waves will be added to climate models as part of this CPT collaboration, to replace ad hoc mixing prescriptions (such as the Gargett 1984 scheme) that are currently used. These processes include dissipation of low-mode internal waves (A. Waterhouse et al. 2012, unpublished manuscript) from scattering at topography (Legg 2012, manuscript submitted to *J. Phys. Oceanogr.*) parametric subharmonic instability (PSI) at critical latitudes (MacKinnon and Winters 2005), nonlinear wave–wave interactions, but also dissipation of lee waves and near

inertial waves (Jochum et al. 2013), and dissipation of internal-waves at tall/steep topography (Legg and Klymak 2008; Klymak et al. 2010). For credible simulations of a changing climate, internal-wave-driven mixing needs to be represented by physically based parameterizations in ocean models, to allow mixing to evolve in space and time depending on the ocean state.

Acknowledgments. The authors thank Stephen Griffies and Maxim Nikurashin for reviewing early versions of this manuscript, Bonnie Samuels for helping to set up the simulations, and the three anonymous reviewers for helpful comments leading to improvements in the manuscript. This work is a component of the Internal-Wave Driven Mixing Climate Process Team funded by the National Science Foundation Grant OCE-0968721 and the National Oceanic and Atmospheric Administration, U.S. Department of Commerce, Award NA08OAR4320752. The statements, findings, conclusions, and recommendations are those of the authors and do not necessarily reflect the views of the National Oceanic and Atmospheric Administration or the U.S. Department of Commerce.

REFERENCES

Alford, M. H., 2001: Internal swell generation: The spatial distribution of energy flux from the wind to mixed layer near-inertial motions. *J. Phys. Oceanogr.,* **31,** 2359–2368.

——, 2003: Energy available for ocean mixing redistributed through long-range propagation of internal waves. *Nature,* **423,** 159–163.

——, and R. Pinkel, 2000: Observations of overturning in the thermocline: The context of ocean mixing. *J. Phys. Oceanogr.,* **30,** 805–832.

——, and Z. Zhao, 2007: Global patterns of low-mode internal-wave propagation. Part I: Energy and energy flux. *J. Phys. Oceanogr.,* **37,** 1829–1848.

——, and Coauthors, 2011: Energy flux and dissipation in Luzon Strait: Two tales of two ridges. *J. Phys. Oceanogr.,* **41,** 2211–2222.

Bell, T. H., 1975: Lee waves in stratified flows with simple harmonic time dependence. *J. Fluid Mech.,* **67,** 705–722.

Bessières, L., G. Madec, and F. Lyard, 2008: Global tidal residual mean circulation: Does it affect a climate OGCM? *Geophys. Res. Lett.,* **35,** L03609, doi:10.1029/2007GL032644.

Bryan, K., and L. Lewis, 1979: A water mass model of the world ocean. *J. Geophys. Res.,* **84,** 2503–2517.

D'Asaro, E., M. Eriksen, M. Levine, P. Niller, C. Paulson, and P. Van Meurs, 1995: Upper-ocean inertial currents forced by a strong storm. Part I: Data and comparisons with linear theory. *J. Phys. Oceanogr.,* **25,** 2909–2936.

Dunne, J. P., and Coauthors, 2012: GFDL's ESM2 global coupled climate–carbon Earth System Models. Part I: Physical formulation and baseline simulation characteristics. *J. Climate,* **25,** 6646–6665.

Egbert, G. D., and S. Y. Erofeeva, 2002: Efficient inverse modeling of barotropic ocean tides. *J. Atmos. Oceanic Technol.,* **19,** 183–204.

——, and R. D. Ray, 2000: Significant dissipation of tidal energy in the deep ocean inferred from satellite altimeter data. *Nature,* **405,** 775–778.

——, and ——, 2001: Estimates of M2 tidal energy dissipation from TOPEX/Poseidon altimeter data. *J. Geophys. Res.,* **106** (C10), 22 475–22 502.

Friedrich, T., A. Timmermann, T. Decloedt, D. S. Luther, and A. Mouchet, 2011: The effect of topography-enhanced diapycnal mixing on ocean and atmospheric circulation and marine biogeochemistry. *Ocean Modell.,* **39,** 262–274.

Gargett, A. E., 1984: Vertical eddy diffusivity in the ocean interior. *J. Mar. Res.,* **42,** 359–393.

Garrett, C., and E. Kunze, 2007: Internal tide generation in the deep ocean. *Annu. Rev. Fluid Mech.,* **39,** 57–87.

Griffies, S. M., R. C. Pacanowski, and R. W. Hallberg, 2000: Spurious diapycnal mixing associated with advection in a z-coordinate ocean model. *Mon. Wea. Rev.,* **128,** 538–564.

Hallberg, R., and A. Adcroft, 2009: Reconciling estimates of the free surface height in lagrangian vertical coordinate ocean models with mode-split time stepping. *Ocean Modell.,* **29,** 15–26, doi:10.1016/j.ocemod.2009.02.008.

Harrison, M. J., and R. W. Hallberg, 2008: Pacific subtropical cell response to reduced equatorial dissipation. *J. Phys. Oceanogr.,* **38,** 1894–1912.

Huang, R. X., 1999: Mixing and energetics of the oceanic thermohaline circulation. *J. Phys. Oceanogr.,* **29,** 727–746.

Ilicak, M., A. Adcroft, S. M. Griffies, and R. Hallberg, 2012: Spurious dianeutral mixing and the role of momentum closure. *Ocean Modell.,* **45-46,** 37–58.

Jackson, L., R. Hallberg, and S. Legg, 2008: A parameterization of shear-driven turbulence for ocean climate models. *J. Phys. Oceanogr.,* **38,** 1033–1053.

Jayne, S. R., 2009: The impact of abyssal mixing parameterizations in an ocean general circulation model. *J. Phys. Oceanogr.,* **39,** 1756–1775.

——, and L. C. St. Laurent, 2001: Parameterizing tidal dissipation over rough topography. *Geophys. Res. Lett.,* **28,** 811–814.

Jochum, M., B. P. Briegleb, G. Danabasoglu, W. G. Large, N. J. Norton, S. R. Jayne, M. H. Alford, and F. O. Bryan, 2013: The impact of oceanic near-inertial waves on climate. *J. Climate,* in press.

Klymak, J. M., and Coauthors, 2006: An estimate of tidal energy lost to turbulence at the Hawaiian ridge. *J. Phys. Oceanogr.,* **36,** 1148–1164.

——, S. A. Legg, and R. Pinkel, 2010: A simple parameterization of turbulent tidal mixing near supercritical topography. *J. Phys. Oceanogr.,* **40,** 2059–2074.

Ledwell, J. R., E. T. Montgomery, K. L. Polzin, L. C. St. Laurent, R. W. Schmitt, and J. M. Toole, 2000: Mixing over rough topography in the Brazil basin. *Nature,* **403,** 179–182.

Legg, S., and J. M. Klymak, 2008: Internal hydraulic jumps and overturning generated by tidal flow over a steep ridge. *J. Phys. Oceanogr.,* **38,** 1949–1964.

——, R. Hallberg, and J. Girton, 2006: Comparison of entrainment in overflows simulated by z-coordinate, isopycnal and non-hydrostatic models. *Ocean Modell.,* **11,** 69–97.

——, and Coauthors, 2009: Improving oceanic overflow representation in climate models: The gravity current entrainment climate process team. *Bull. Amer. Meteor. Soc.,* **90,** 657–670.

Levitus, S., and Coauthors, 1998: *Introduction.* Vol. 1, *World Ocean Database 1998,* NOAA Atlas NESDIS 18, 346 pp.

MacKinnon, J. A., and K. B. Winters, 2005: Subtropical catastrophe: Significant loss of low-mode tidal energy at 28.9°. *Geophys. Res. Lett.,* **32,** L15605, doi:10.1029/2005GL023376.

Melet, A., J. Verron, and J.-M. Brankart, 2012: Potential outcomes of glider data assimilation in the Solomon Sea: Control of the water mass properties and parameter estimation. *J. Mar. Syst.,* **94,** 232–246, doi:10.1016/j.jmarsys.2011.12.003.

Munk, W., and C. Wunsch, 1998: Abyssal recipes II: Energetics of tidal and wind mixing. *Deep-Sea Res.,* **45,** 1977–2010.

Nikurashin, M., and S. Legg, 2010: A mechanism for local dissipation of internal tides generated at rough topography. *J. Phys. Oceanogr.,* **41,** 378–395.

——, and R. Ferrari, 2011: Global energy conversion rate from geostrophic flows into internal lee waves in the deep ocean. *Geophys. Res. Lett.,* **38,** L08610, doi:10.1029/2011GL046576.

Niwa, Y., and T. Hibiya, 2001: Numerical study of the spatial distribution of the M2 internal tide in the Pacific Ocean. *J. Geophys. Res.,* **106** (C10), 22 441–22 449.

Osborn, T. R., 1980: Estimates of the local rate of vertical diffusion from dissipation measurements. *J. Phys. Oceanogr.,* **10,** 83–89.

Polzin, K. L., 2004: Idealized solutions for the energy balance of the finescale internal wave field. *J. Phys. Oceanogr.,* **34,** 231–246.

——, 2009: An abyssal recipe. *Ocean Modell.,* **30,** 298–309, doi:10.1016/j.ocemod.2009.07.006.

——, J. M. Toole, J. R. Ledwell, and R. W. Schmitt, 1997: Spatial variability of turbulent mixing in the abyssal ocean. *Science,* **276,** 93–96.

Saenko, O. A., and W. J. Merryfield, 2005: On the effect of topographically enhanced mixing on the global ocean circulation. *J. Phys. Oceanogr.,* **35,** 826–834.

Scott, J. R., and J. Marotzke, 2002: The location of diapycnal mixing and the meridional overturning circulation. *J. Phys. Oceanogr.,* **32,** 3578–3595.

Simmons, H. L., S. R. Jayne, L. C. St. Laurent, and A. J. Weaver, 2004: Tidally driven mixing in a numerical model of the ocean general circulation. *Ocean Modell.,* **6** (3–4), 245–263, doi:10.1016/S1463-5003(03)00011-8.

Smith, W. H. F., and D. T. Sandwell, 1997: Global sea floor topography from satellite altimetry and ship depth soundings. *Science,* **277,** 1956–1962.

St. Laurent, L. C., and C. Garrett, 2002: The role of internal tides in mixing the deep ocean. *J. Phys. Oceanogr.,* **32,** 2882–2899.

——, and J. D. Nash, 2004: An examination of the radiative and dissipative properties of deep ocean internal tides. *Deep-Sea Res. II,* **51,** 3029–3042.

——, H. L. Simmons, and S. R. Jayne, 2002: Estimating tidally driven mixing in the deep ocean. *Geophys. Res. Lett.,* **29,** 2106, 10.1029/2002GL015633.

Thurnherr, A. M., L. C. St. Laurent, K. G. Speer, J. M. Toole, and J. R. Ledwell, 2005: Mixing associated with sills in a canyon on the midocean ridge flank. *J. Phys. Oceanogr.,* **35,** 1370–1381.

Wunsch, C., and R. Ferrari, 2004: Vertical mixing, energy and the general circulation of the oceans. *Annu. Rev. Fluid Mech.,* **36,** 281–314.